gebiology

Geobiology (2016) DOI: 10.1111/gbi.12182

Oceanic oxygenation events in the anoxic Ediacaran ocean

S. K. SAHOO,[1] N. J. PLANAVSKY,[2] G. JIANG,[1] B. KENDALL,[3] J. D. OWENS,[4] X. WANG,[5] X. SHI,[5] A. D. ANBAR[6] AND T. W. LYONS[7]

[1]*Department of Geoscience, University of Nevada, Las Vegas, NV, USA*
[2]*Department of Geology and Geophysics, Yale University, New Haven, CT, USA*
[3]*Department of Earth and Environmental Sciences, University of Waterloo, Waterloo, ON, Canada*
[4]*Department of Earth, Ocean and Atmospheric Science, Florida State University, Tallahassee, FL, USA*
[5]*School of Earth Science and Resources, China University of Geosciences, Beijing, China*
[6]*Department of Chemistry and Biochemistry, School of Earth and Space Exploration, Arizona State University, Tempe, AZ, USA*
[7]*Department of Earth Sciences, University of California, Riverside, CA, USA*

ABSTRACT

The ocean-atmosphere system is typically envisioned to have gone through a unidirectional oxygenation with significant oxygen increases in the earliest (ca. 635 Ma), middle (ca. 580 Ma), or late (ca. 560 Ma) Ediacaran Period. However, temporally discontinuous geochemical data and the patchy metazoan fossil record have been inadequate to chart the details of Ediacaran ocean oxygenation, raising fundamental debates about the timing of ocean oxygenation, its purported unidirectional rise, and its causal relationship, if any, with the evolution of early animal life. To better understand the Ediacaran ocean redox evolution, we have conducted a multi-proxy paleoredox study of a relatively continuous, deep-water section in South China that was paleogeographically connected with the open ocean. Iron speciation and pyrite morphology indicate locally euxinic (anoxic and sulfidic) environments throughout the Ediacaran in this section. In the same rocks, redox sensitive element enrichments and sulfur isotope data provide evidence for multiple oceanic oxygenation events (OOEs) in a predominantly anoxic global Ediacaran–early Cambrian ocean. This dynamic redox landscape contrasts with a recent view of a redox-static Ediacaran ocean without significant change in oxygen content. The duration of the Ediacaran OOEs may be comparable to those of the oceanic anoxic events (OAEs) in otherwise well-oxygenated Phanerozoic oceans. Anoxic events caused mass extinctions followed by fast recovery in biologically diversified Phanerozoic oceans. In contrast, oxygenation events in otherwise ecologically monotonous anoxic Ediacaran–early Cambrian oceans may have stimulated biotic innovations followed by prolonged evolutionary stasis.

Received 08 December 2015; accepted 06 February 2016

Corresponding author: G. Jiang. Tel.: +1 702 895 2708; fax: +1 702 895 4064; e-mail: Ganqing.Jiang@unlv.edu

INTRODUCTION

The Ediacaran Period (635–541 Ma) is generally thought to mark a fundamental shift in Earth's surface redox state (Canfield *et al.*, 2007; Och & Shields-Zhou, 2012; Lyons *et al.*, 2014) and encompasses the emergence of complex ecosystems (Sperling *et al.*, 2013; Xiao, 2014; Droser & Gehling, 2015). Metazoans first appeared in the earliest Ediacaran (Yin *et al.*, 2007) or during the Cryogenian (Love *et al.*, 2009; Erwin *et al.*, 2011), yet evidence of animals with energy-expensive and O_2-demanding lifestyles, such as motility and predation, appear much later in the fossil record (≤590–558 Ma; Narbonne, 2004, 2005; Xiao & Laflamme, 2009; Pecoits *et al.*, 2012; Chen *et al.*, 2014; Droser & Gehling, 2015). This pattern of an early appearance but late ecological diversification may be tied to shifts in the oxidizing capacity of Earth's surface throughout the Ediacaran and early Cambrian (Knoll & Carroll, 1999; Knoll, 2011; Chen *et al.*, 2015a).

Currently, there are seemingly contradictory views of the Ediacaran marine redox evolution. Several records suggest ocean oxygenation around or after 580 Ma, the

time period following the last of the major Neoproterozoic glaciations (Canfield *et al.*, 2007; Scott *et al.*, 2008). More recently, it has been argued that ocean oxygenation became pervasive during the earliest Ediacaran (ca. 635–630 Ma), in the immediate aftermath of the Marinoan glaciation (Sahoo *et al.*, 2012). Both of these views seemly conflict with evidence for generally persistent, widespread anoxic conditions (Canfield *et al.*, 2008; Li *et al.*, 2010; Sperling *et al.*, 2015) and with a lack of evidence of ocean ventilation in some Ediacaran basins (Johnston *et al.*, 2013). Further, most of the Ediacaran seems to be a time period in which iron is commonly the anoxic water column or pore-water redox buffer (ferruginous conditions), instead of sulfide. Ferruginous oceans are a common feature in Earth's early history (Poulton & Canfield, 2011), when generally reducing conditions prevailed, but is extremely rare in well-oxygenated sulfate-rich oceans.

A new, stratigraphically more continuous window into Ediacaran marine redox conditions is needed to reconcile apparently conflicting views about the Ediacaran redox evolution. In this paper, we report a multi-proxy study that constrains local and global redox conditions of the Ediacaran ocean from a deep-water section at Wuhe, South China (Fig. 1). The Wuhe section is ideally suited for tracking the Ediacaran ocean redox evolution because (1) it was paleogeographically located in the slope of the Ediacaran Yangtze platform (Fig. 1B,C; Jiang *et al.*, 2011), a passive margin developed in the southeastern side of the Yangtze Block (YB) that was well connected with the open ocean during the Ediacaran–early Cambrian (Fig. 1A; Jiang *et al.*, 2003; Zhang *et al.*, 2013, 2015), and (2) relatively complete Ediacaran strata in this section are enriched in black shales that allow currently available redox proxies to capture paleoceanographic signals.

STRATIGRAPHY AND AGE CONSTRAINTS

The Wuhe section (N 26°45′93.6″, E 108°25′0.5″) in Guizhou Province crops out along the Qingshui River in Taijiang County. The section includes the Doushantuo (120 m), the Dengying (12 m), and the Liuchapo (40 m) formations and a few meters of the basal Niutitang Formation (Figs 1D and 2). The Doushantuo Formation can be divided into four distinct members (Members I–IV) that are roughly correlatable with those in the Yangtze Gorges area (Fig. 1D; Jiang *et al.*, 2011). The base of the Doushantuo Formation consists of a 2.3-m-thick cap carbonate (Member I) that overlies the glacial diamictite of the Nantuo Formation and serves as a marker for regional stratigraphic correlation (Jiang *et al.*, 2006). The top of the Doushantuo Formation is characterized by 5-m-thick, organic-rich black shales with sparse fist-sized phosphatic-pyrite nodules (Member IV). This black shale interval is also a distinctive marker across the Ediacaran Yangtze platform and is correlatable with the Member IV black shales in the Yangtze Gorges area. The majority of the Doushantuo Formation consists of laminated black shales with subordinate micritic or microcrystalline dolostone and a few layers of olistostrome dolostone breccias (Members II and III). In the middle of the Doushantuo Formation, a thick (2.5–4 m) dolostone breccia layer may record a regional stratigraphic discontinuity that has been tentatively correlated across the Yangtze platform (Jiang *et al.*, 2007, 2011). This interval also marks the Member II and III boundary (Figs 1D and 2) in this section.

The 12-m-thick Dengying Formation in this section is composed of micritic-microcrystalline dolostone with lenticular chert beds or nodules. This unit is most likely time-equivalent to the lowermost portion (Hamajing Member) of the Dengying Formation in the Yangtze Gorges area (Jiang *et al.*, 2007, 2011; Zhu *et al.*, 2007). The overlying Liuchapo Formation, which consists of 40-m-thick bedded cherts with thin black shale interbeds, is overlain by phosphatic organic-rich black shales of the Niutitang Formation (or Jiumenchong Formation in local stratigraphic terms). Only a few meters of the basal Niutitang Formation is continuously exposed in this section. There are sponge spicules and trilobites in the Niutitang confirming a Cambrian age.

Based on the distinctive marker beds and regional stratigraphic correlation, the base of the Doushantuo Formation is reasonably assigned an age of ca. 635 Ma (Fig. 1D; Condon *et al.*, 2005). The top of the Doushantuo Formation was previously thought to be ca. 551 Ma. Recent studies, however, indicate that the age of 551.1 ± 0.7 Ma from the top of the Miaohe Member in the Yangtze Gorges area (Condon *et al.*, 2005; Zhang *et al.*, 2005) may be much younger than the Doushantuo Member IV black shales (An *et al.*, 2015). With this new update, the age of the Doushantuo Member IV is estimated as ca. 560 Ma (Fig. 1D; An *et al.*, 2015). Regional stratigraphic analyses correlated the Member II–Member III boundary with a regional stratigraphic discontinuity in shallow-water facies (Jiang *et al.*, 2011). If this regional discontinuity recorded a sea-level fall event, it might be time-equivalent with the Gaskiers glaciation at ca. 580 Ma. The Liuchapo–Niutitang boundary was traditionally considered as the Ediacaran–Cambrian (E–C) boundary, but recent U–Pb ages of 522.7 ± 4.9 Ma (Wang *et al.*, 2012a) and 522.3 ± 3.7 Ma (Chen *et al.*, 2015b) from the basal Niutitang Formation suggested that the E–C boundary is located within the Liuchapo Formation, which is now confirmed by the age of 542.6 ± 3.7 Ma a few meters below the Liuchapo–Niutitang boundary (Chen *et al.*, 2015b).

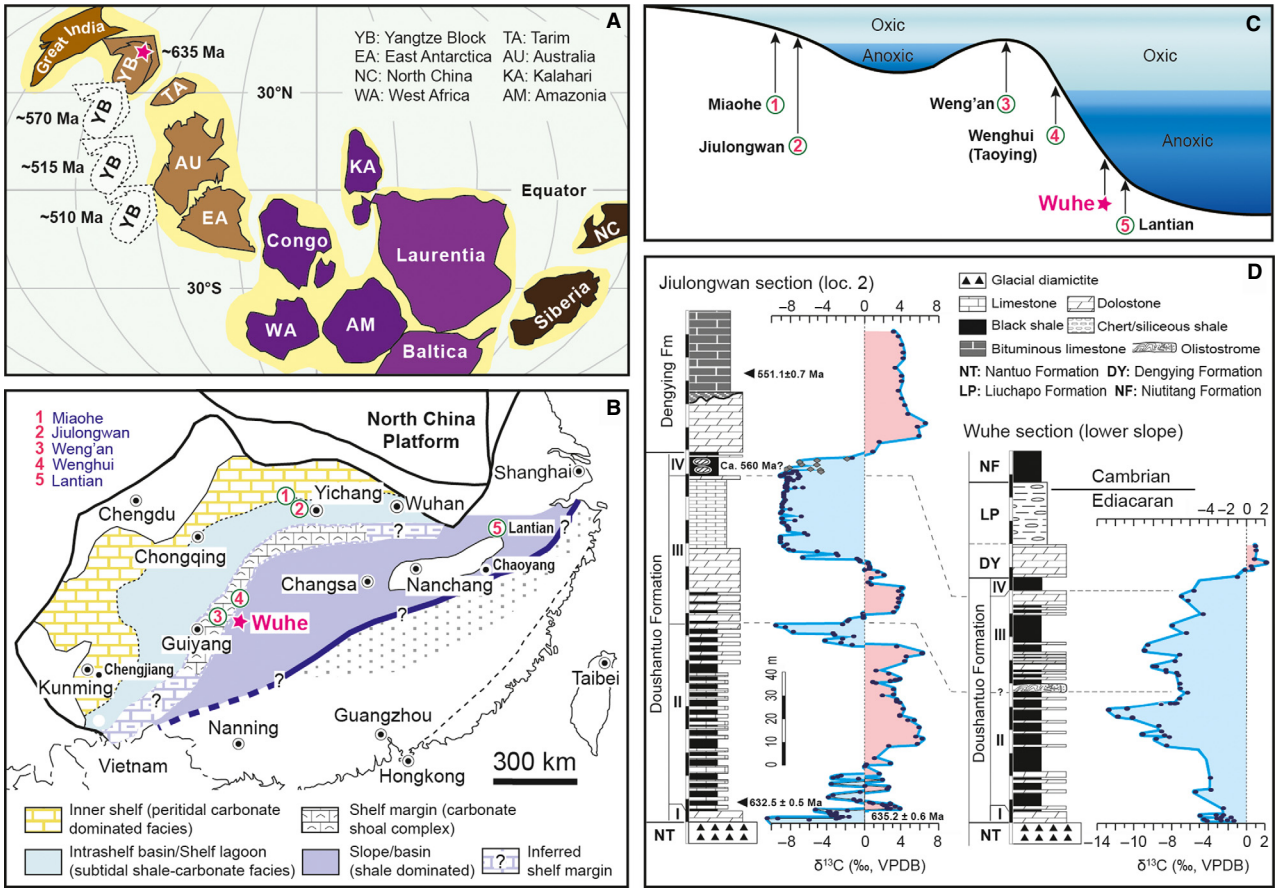

Fig. 1 Paleogeographic location of the Wuhe section in South China and its correlation with the shelf section in the Yangtze Gorges area. (A) Location of the Yangtze Block (YB) in global reconstruction at ca. 635 Ma (Zhang *et al.*, 2013) and its latitudinal change from ca. 635 to ca. 510 Ma (dashed outlines; Zhang *et al.*, 2015). Existing paleomagnetic data indicate that the YB was most likely an independent continent block well connected with the open ocean during the Ediacaran–early Cambrian (Zhang *et al.*, 2015). (B and C) Paleogeographic location of the Wuhe section on the Ediacaran Yangtze platform (modified from Jiang *et al.*, 2011). Circled red-color numbers in both B and C mark the location of sections where representative Ediacaran biotas were reported. (D) Stratigraphic correlation of the Doushantuo and lower Dengying formations between Jiulongwan (shelf) and Wuhe (slope) sections. U–Pb ages are from Condon *et al.* (2005) and the stratigraphic position of the 551.1 ± 0.7 Ma age has been adjusted according to An *et al.* (2015). Carbon isotope data are from Jiang *et al.* (2007).

SAMPLES AND ANALYTICAL METHODS

Samples were collected at an average spacing of 20–50 cm (depending on the availability of black shales) along the eastern side of the Qingshui River in a dry season when part of the river channel was exposed, leaving fresh and clean outcrops. Large samples (0.5–1 kg) were collected from the field, and they were cut into slabs before powdering. Only the center part of samples without macroscopic pyrites was used for chemical analyses.

Major and trace elemental abundances, iron speciation, and total organic carbon (TOC) were mostly analyzed at the Biogeochemistry Lab at the University of California, Riverside (UCR). A portion of the samples were analyzed at the W. M. Keck Foundation Laboratory for Environmental Biogeochemistry, Arizona State University (ASU). Sample preparation and analyses follow previously published methods (Poulton & Canfield, 2005; Scott *et al.*, 2008; Kendall *et al.*, 2010; Li *et al.*, 2010).

Major and trace element concentrations

Powdered sample splits were ashed for 8–10 h at 550 °C and dissolved by HF-HNO_3-HCl acid digestion. Trace and major element concentrations were determined on a ThermoFinnigan X-Series (ASU) and Agilent 7500E (UCR) quadrupole ICP-MS (inductively coupled plasma mass spectrometry). Accuracy and precision were monitored with duplicate samples and the US Geological Survey Devonian black shale standard SDO-1. Analytical reproducibility in individual runs was within 5% for the presented elements.

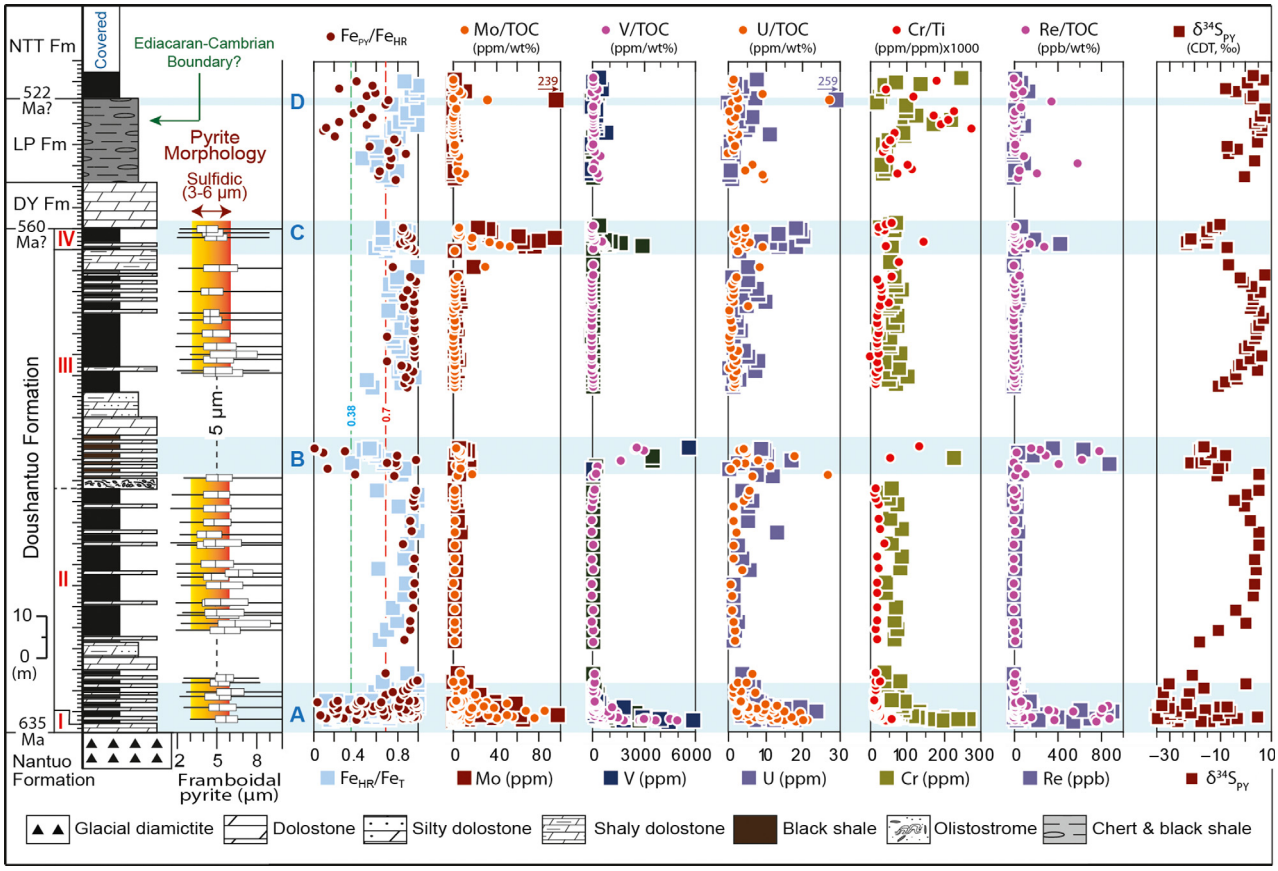

Fig. 2 Geochemical profiles of the Ediacaran and early Cambrian strata from the Wuhe section, South China (data are included in Table S1). The box-and-whisker plots of pyrite framboid diameters (PFD) show the median (5 µm), range, and 25th and 75th percentiles of PFD distributions (Wang *et al.*, 2012b). The PFD and iron speciation data ($Fe_{HR}/Fe_T > 0.38$; $Fe_{PY}/Fe_{HR} > 0.7$) indicate persistent water-column euxinia during most of the Ediacaran, making this section ideal for tracking the global ocean redox evolution using RSE enrichments. Highly enriched RSE (Mo, V, U, Cr, Re) in the basal (Zone A), middle (Zone B), and uppermost (Zone C) Doushantuo Formation are interpreted as recording three distinctive oxygenation events at ca. 635, ca. 580, and ca. 560 Ma. Crustal-level RSE values between these events record a return to prolonged oceanic anoxia. This interpretation is supported by low $\delta^{34}S_{PY}$ values during oxygenation events and high $\delta^{34}S_{PY}$ values in between. The late Ediacaran–early Cambrian strata (ca. 560–522 Ma) in this section is strongly condensed and the upper Liuchapo Formation show sparse enriched Cr and Re and low $\delta^{34}S_{PY}$ values, but their temporal trend is obscured possibly due to insufficient sampling and/or non-sulfidic shales that did not capture the Mo, U, and V signals. RSE enrichments and low $\delta^{34}S_{PY}$ values are also seen at the basal Niutitang Formation (Zone D), which has been recently updated in a paleogeographically adjacent section at Hejiapu (Wang *et al.*, 2015).

Iron speciation

Biogeochemically highly reactive iron (Fe_{HR}) is defined as pyrite iron (Fe_{PY}) plus other iron phases that are potentially reactive with hydrogen sulfide on diagenetic time scales: carbonate-associated iron (Fe_{Carb}), ferric oxides (Fe_{Ox}), and magnetite (Fe_{Mag}). Hence, highly reactive iron can be expressed as $Fe_{HR} = Fe_{PY} + Fe_{Carb} + Fe_{Ox} + Fe_{Mag}$ (Poulton & Canfield, 2005; Canfield *et al.*, 2007). Fe_{PY} was calculated (assuming a stoichiometry of FeS_2) from the weight percentage of sulfur extracted during a 2 h hot chromous chloride distillation followed by iodometric titration. Other iron species—Fe_{Carb}, Fe_{Ox}, and Fe_{Mag}—were extracted sequentially using sodium acetate solution, dithionite solution, and ammonium oxalate, respectively. The sequential extracts were analyzed with an Agilent 7500ce ICP-MS. Total iron concentrations (Fe_T) were determined by HF-HNO_3-HCl acid digestion followed by ICP-MS analysis. Analytical reproducibility of iron measurements, monitored by duplicate analyses within and between sample batches, was typically within 5%, with the exception of a few unusually low-Fe (≤0.1 wt%) samples.

Sulfur isotopes

Pyrite sulfur was extracted for isotope measurements using chromous chloride distillation and re-precipitation as Ag_2S. Sulfur isotope measurements were made with a ThermoFinnigan Delta V continuous-flow stable-isotope-ratio mass spectrometer at UCR. Sulfur isotope data are reported as per mil (‰) deviations from the isotope

composition of Vienna Cañon Diablo Troilite (VCDT). Analytical precision is better than 0.2‰ on the basis of single-run and long-term standard monitoring.

Organic carbon concentration

Total organic carbon (TOC) contents were determined by taking the difference between carbonate-carbon liberated by 4M HCl and total carbon released by combustion at 1400 °C, both of which were measured with an ELTRA C/S determinator at UCR. Analytical precision for TOC monitored by duplicates is better than 0.1%.

Mo and U enrichment factors

Authigenic Mo and U enrichment factors (EFs) are calculated with the equation $X_{EF} = [(X/Al)_{sample}/(X/Al)_{PAAS}]$ (Tribovillard *et al.*, 2006; Algeo & Tribovillard, 2009), where X and Al refer to their weight concentrations (ppm for Mo, U and weight percent for Al). PAAS (post-Archean average shale) data for normalization are from McLennan (2001).

REDOX PROXIES

We use the well-established, empirically calibrated Fe speciation proxy data to identify local water column redox conditions. These inferred local conditions then provide the background for our interpretations of regional/global marine redox based on RSE and sulfur isotope geochemistry. Black shales with $Fe_{HR}/Fe_T > 0.38$ are indicative of Fe scavenging under an anoxic water column (Poulton & Canfield, 2011). Similarly, Fe_T/Al ratios greater than 0.5 in continental margin sediments is an indicator of water column anoxia (Lyons & Severmann, 2006). Anoxic shales with $Fe_{PY}/Fe_{HR} > 0.7$–0.8 are considered to represent deposition under euxinic conditions, whereas $Fe_{PY}/Fe_{HR} < 0.7$ represents ferruginous conditions (Poulton & Canfield, 2011). Independent evidence of euxinic conditions come from pyrite framboid diameters (PFD) that are consistently less than 10 μm (Wilkin *et al.*, 1997; Wang *et al.*, 2012b).

If black shales can be independently determined to have been deposited under locally euxinic conditions, the degree of RSE enrichments (Mo, U, Re, V, Cr) can be used to track first order shifts in the global marine redox state (Emerson & Huested, 1991; Algeo & Lyons, 2006; Lyons *et al.*, 2009). This idea builds from two key principles: (1) the global marine redox landscape is the primary control on the size of the dissolved oceanic RSE reservoir (Emerson & Huested, 1991) and (2) the RSE reservoir exerts a first order control on RSE enrichments in euxinic sediments (Algeo & Lyons, 2006; Lyons *et al.*, 2009). This approach is most clearly illustrated in euxinic sections that capture Phanerozoic Oceanic Anoxic Events: large drops in RSE enrichments correspond to the peak of anoxic conditions on a global scale (Hetzel *et al.*, 2009; Owens *et al.*, 2012). Sulfur isotopes complement the Fe and RSE proxies by providing a means to track the global redox controlled sulfur (pyrite) burial fluxes and local sulfur redox transformations (Lyons *et al.*, 2009; Scott *et al.*, 2014; Gomes & Hurtgen, 2015).

RESULTS

At the Wuhe section (Fig. 2 and Table S1), the Doushantuo Formation shows a marked enrichment in Fe_{HR}/Fe_T ratios (0.72 ± 0.19) and extremely low levels of ferric oxides (0.07 ± 0.18). Through most of the section, Fe_T/Al ratios (0.52 ± 0.21) are elevated relative to typical continental margin sediments. The Fe_{PY}/Fe_{HR} ratios (0.87 ± 0.13) are consistently high, and there is a strong correlation ($R^2 = 0.91$) between Fe_{HR} and Fe_{PY}. Further, the entire succession is characterized by abundant small diameter pyrite framboids (mean PFD = 5.4 ± 0.6 μm; $n = 5274$; Wang *et al.*, 2012b).

There are three discrete intervals (ca. 635 Ma basal Member II, ca. 580 Ma basal Member III, and ca. 560 Ma Member IV) with high Mo, V, Cr, Re, and U enrichments (Fig. 2). High RSE values (1–172 ppm of Mo, 10^2–10^4 ppm of V, 3–16 ppm of U, 4–700 ppb of Re, and 25–201 ppm of Cr) and low $\delta^{34}S_{PY}$ values down to –34.6‰ (Fig. 2; Zone A) occur in basal Member II, followed by a progressive shift to low, crustal RSE concentrations (2–5 ppm of Mo, 80–100 ppm of V, 3–5 ppm of U, 3–46 ppb of Re, and 34–88 ppm of Cr) and a shift to high $\delta^{34}S_{PY}$ values (from –35‰ to +6‰) spanning from 10 to 60 m. At the base of Member III, we again observe high RSE values (7–15 ppm of Mo, 10^2–10^4 ppm of V, 16–19 ppm of U, 10–10^3 ppb of Re, and 230–1422 ppm of Cr) and low $\delta^{34}S_{PY}$ values down to –21.5‰ (Fig. 2; Zone B). Shortly after this metal enrichment zone, RSE values again decrease up section to near crustal levels, and $\delta^{34}S_{PY}$ increases up to +6‰ in middle-upper Member III. Lastly, in Member IV there is a third positive shift (Fig. 2; Zone C) of RSE enrichments (2–126 ppm of Mo, 10^1–10^4 ppm of V, 3–32 ppm of U, 10–10^3 ppb of Re, and 28–508 ppm of Cr) and a decrease of $\delta^{34}S_{PY}$ down to –23.3‰.

The overlying Liuchapo Formation witnesses another drop in RSE values and increase in $\delta^{34}S_{PY}$. A few high Cr and Re values and low $\delta^{34}S_{PY}$ values are also observed in the middle and upper Liuchapo Formation, but a clear temporal pattern is not observed. However, the Fe speciation data in this interval should be viewed with caution because most of the samples are siliceous shales with $Fe_T < 1\%$. Metal enrichments are likely influenced by the general lack of sulfidic shales in this interval (for Mo in

particular, $Fe_{PY}/Fe_{HR} < 0.7$; Fig. 2) and/or insufficient sample resolution, given that the Liuchapo Formation is strongly condensed at this locality (~40 Ma for a 40-m-thick interval). High RSE values and low $\delta^{34}S_{PY}$ values are observed at the basal Niutitang Formation (Zone D; Fig. 2), which are better expressed in a paleogeographically adjacent section at Hejiapu where more sulfidic black shales are present (Wang *et al.*, 2015).

DISCUSSION

Paleogeographic context for ocean redox interpretation

In the modern oxygenated ocean, only euxinic shales in marine basins with access to the open ocean effectively capture the high dissolved RSE concentrations in seawater (Algeo & Lyons, 2006; Lyons & Severmann, 2006; Lyons *et al.*, 2009). In ancient marine sedimentary successions, high RSE enrichments comparable to those of the modern euxinic shales (such as Zone A, B, C, and D in Fig. 2) provide strong evidence for high dissolved RSE concentrations in a broadly oxygenated ocean (Scott *et al.*, 2008; Kendall *et al.*, 2010; Och & Shields-Zhou, 2012; Sahoo *et al.*, 2012; Reinhard *et al.*, 2013; Large *et al.*, 2014). However, low RSE values from a particular stratigraphic unit would have much less definitive meaning and could be resulted from (1) low RSE enrichments in oxic/suboxic local environments (comparable to modern oxic/suboxic sediments), (2) strong basin restriction (isolation), or (3) low dissolved RSE concentrations in poorly oxygenated ocean. We eliminate option 1 as a likely possibility because iron speciation and pyrite morphology data from the Wuhe section (Fig. 2) document persistently euxinic local environments through most of the Ediacaran. Persistent euxinia makes sense given that the Wuhe section was located paleogeographically on the middle-lower slope of the Ediacaran Yangtze platform (Jiang *et al.*, 2007, 2011) where upwelling and high primary productivity may have fostered oxygen deficiency and sulfate reduction. The euxinic Wuhe black shales with high Fe_{PY}/Fe_{HR} values (>0.7–0.8) and small (3–6 μm) PDFs demonstrate that the majority of low RSE values from the section (Fig. 2) are not a consequence of ineffective trapping of RSEs in oxic/suboxic water column. However, the redox state of the Liuchapo Formation and some data points in Zones A and B (Fig. 2) have low (<0.7) Fe_{PY}/Fe_{HR} values, suggesting non-euxinic conditions.

It is more difficult during the Proterozoic, relative to younger intervals, to gauge the extent of basin restriction and to determine if the extent of basin isolation might have dramatically lowered water column RSE concentrations. Due to basin restriction, deep-water Mo concentrations in the modern Black Sea are as low as 4 nmol/kg, compared to ~103 nmol/kg in the open ocean (Algeo & Lyons, 2006). Previous paleoredox studies of the Doushantuo Formation in the Yangtze Gorges area (Jiulongwan section; loc. 2 in Fig. 1B–D), which was located in a paleogeographically restricted shelf lagoon setting (Jiang *et al.*, 2011), documented unusually low RSE values (Bristow *et al.*, 2009; Li *et al.*, 2010). The exceptional values from this location were high RSE concentrations from the top of the Doushantuo Formation (Member IV; Scott *et al.*, 2008; Kendall *et al.*, 2015). On this basis, Och *et al.* (2015) interpreted the low RSE values from the Ediacaran succession in South China as reflecting basin restriction in the Nanhua basin, while high RSE values at the base and top of the Doushantuo Formation (Scott *et al.*, 2008; Sahoo *et al.*, 2012) and Ediacaran–Cambrian transition (e.g., Guo *et al.*, 2007) record open-ocean signatures associated with major transgressive events. This interpretation implies that the open ocean was irreversibly oxygenated and had high RSE concentrations since the beginning of the Ediacaran period, which contradicts with the lack of any other evidence for broad and persistent ocean ventilation and evidence, to the contrary, for widespread anoxia in other sedimentary basins (e.g., Johnston *et al.*, 2013; Sperling *et al.*, 2015).

Most of the data in Och *et al.* (2015) are from the Yangtze Gorges area where basin restriction in an intrashelf lagoon is likely, or from short segments of the slope-basin sections where sparse data points are insufficient to show clear temporal RSE trends. In contrast, the Wuhe section data reported here provide the most temporally continuous Ediacaran redox record to date from a deep-water section likely connected with the open ocean. Paleomagnetic data and global reconstruction indicated that during the Ediacaran and early Cambrian, South China did not attach to any other major continent and was an independent continental block surrounded by oceans (Fig. 1A; Jiang *et al.*, 2003; Zhang *et al.*, 2013, 2015). Carbon (Jiang *et al.*, 2007; Zhou & Xiao, 2007; Zhu *et al.*, 2007, 2013; Tahata *et al.*, 2012) and strontium (Sawaki *et al.*, 2010; Cui *et al.*, 2015) isotope profiles and the marine fossil record (Zhou *et al.*, 2007; Liu *et al.*, 2013) from the Doushantuo Formation are also comparable with those of the global successions, suggesting marine environments in general. The coherent, gradual temporal $\delta^{34}S_{PY}$ trends from the Wuhe section (Fig. 2) also support an open-marine signal, in contrast with scattered $\delta^{34}S_{PY}$ values from restricted, shelf-lagoon sections in the Yangtze Gorges area (e.g., loc. 2 in Fig. 1B–D; Mcfadden *et al.*, 2008). Despite disagreements about the Neoproterozoic paleogeography, there is compelling evidence that the marine basin along the southeast side of the Yangtze Block was connected to the open ocean. Local restriction in the proximal intrashelf basin was likely (Jiang *et al.*, 2011), but the slope-basin environments, where the Wuhe section was located, should have been well-connected with the global ocean.

The ratio of Mo and U enrichment factors (EFs) may also fingerprint the open ocean connection of the Wuhe section. Because Mo sinks more efficiently than U in sulfidic environments, restricted basins without open-ocean connection would have very low Mo/U ratios in the water column and in sediments (Algeo & Tribovillard, 2009). For example, in the modern Black Sea, the deep watermass has aqueous Mo/U ratios only ~4% of the open ocean seawater (Mo/U ≈ 7.5–7.9) and sediments are significantly depleted in Mo (relative to U). The Mo/U ratios of Zones A, B, and C exceed or are close to those of the modern seawater, except for a few outliers from non-sulfidic samples of Zones A and B (Fig. 3). More importantly, the Mo/U ratios of samples between Zones A, B, and C show a consistent covariation pattern that is comparable with but lower than the molar Mo/U ratio of modern seawater (1 × SW). This trend is typically interpreted as providing a signal for the occurrence of locally euxinic bottom water and unrestricted exchange between local depositional environments and the open ocean (Algeo & Tribovillard, 2009). However, caution should be used when applying this proxy to Pre-cambrian setting, given that U and Mo have different behaviors in ferruginous settings.

Ediacaran oceanic oxygenation events (OOEs)

Based on the Fe proxies and PFDs, the Wuhe section was deposited under near-persistent euxinic conditions throughout the Ediacaran. Further, the abundance of small diameter framboidal pyrites and a lack of Fe oxides indicate limited, if any, late stage sulfide mineralization or oxic alteration. This environmental context, coupled with the lack of obvious evidence for shifts in the degree of basin isolation, sets the stage for using the degree of RSE enrichments to track the evolution of Ediacaran global marine redox landscape.

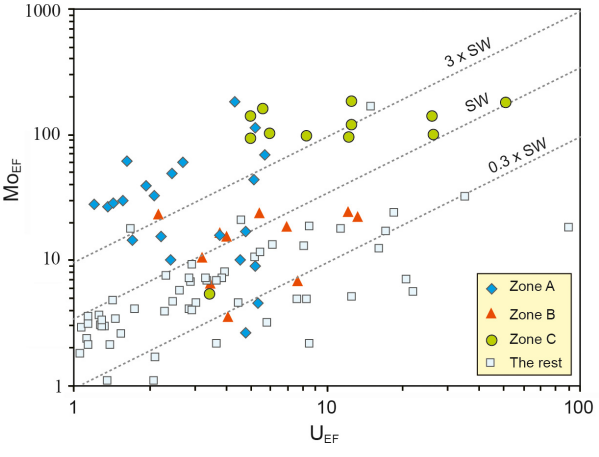

Fig. 3 Mo EF vs. U EF for the Wuhe section black shales. The dashed lines are equivalent to the molar Mo/U ratio for modern seawater (1 × SW), higher than seawater (3 × SW) and for a fraction of modern seawater (0.3 × SW), following Algeo & Tribovillard (2009).

The periods with substantial RSE enrichments indicate the presence of large marine RSE reservoirs and thus a widely oxygenated ocean. Again, this idea builds from the notion that RSE reservoirs are controlled by the extent of anoxia/euxinia on a global scale and that RSE enrichments in anoxic shales track the size of the oceanic RSE reservoir (Emerson & Huested, 1991; Algeo & Lyons, 2006; Hetzel *et al.*, 2009; Lyons *et al.*, 2009; Sahoo *et al.*, 2012; Reinhard *et al.*, 2013). The RSE enrichments at ca. 635, ca. 580, and ca. 560 Ma are comparable to the levels found in Phanerozoic euxinic shales (Scott *et al.*, 2008; Och & Shields-Zhou, 2012; Sahoo *et al.*, 2012), which intuitively suggest comparable marine redox conditions—that is, widespread oxic conditions. In contrast to these relatively thin enriched zones, crustal (majority of Member II) or near-crustal (majority of Member III) RSE values through most of the persistently anoxic Wuhe black shale section indicate that the Ediacaran was characterized, perhaps dominantly so, by intervals of expansive and persistent euxinia and potentially ferruginous conditions. Critically, the persistence of local anoxic conditions at Wuhe allows us, from metal enrichment patterns at a single location, to make inferences about the metal reserves and thus the predominant redox conditions in the global ocean.

Recent modeling efforts suggest that at least 1–10% seafloor euxinia and ≥30% seafloor anoxia are needed to crash the Mo and Cr seawater reservoirs, respectively, to levels that favor near-crustal concentrations in euxinic shales (Reinhard *et al.*, 2013). Thus, the coupled Fe proxy and RSE trends presented here document, for the first time, multiple oxygenation events in an overall anoxic Ediacaran ocean from a single stratigraphic succession, providing unequivocal evidence for large-scale shifts in marine redox conditions.

The large $\delta^{34}S_{PY}$ variations at the Wuhe section, despite evidence for persistent water column pyrite formation from the Fe proxies and PFD record, also suggest dynamic Ediacaran redox conditions. Heavy $\delta^{34}S_{PY}$ values may be linked to decreases in the marine sulfate reservoir, which could be driven by widespread expansion of euxinic conditions and increased global pyrite burial (Scott *et al.*, 2014). Despite the preference for the light sulfur isotope (^{32}S) during microbial sulfate reduction, sulfate–pyrite sulfur isotope fractionations become muted under limited sulfate supplies—thus resulting in isotopically heavy (^{34}S-enriched) pyrite. In addition to these reservoir effects, it is possible that the size of the seawater sulfate reservoir decreased to the extent that combined instantaneous (Scott *et al.*, 2014) and reservoir size effects (cf. Gomes & Hurtgen, 2015) during microbial sulfate reduction generated isotopically heavy pyrites. Alternatively, shifts in $\delta^{34}S_{PY}$ could be tied to variations in the areal extent and depth of oxic

conditions in the surface water column offshore of the Yangtze platform. A decrease in the extent of oxic water column respiration would result in an increase in microbial sulfate reduction rates by favoring delivery of more labile organic matter to anoxic waters. This shift in rates would ultimately decrease the sulfur isotope fractionation ($\Delta^{34}S$) and increase $\delta^{34}S_{PY}$ values (Leavitt *et al.*, 2013). All these factors, individually or working together, require temporally dynamic redox conditions to explain the striking observed trend in $\delta^{34}S$ of pyrites—that is, heavy $\delta^{34}S$ values coincident with low metal enrichments and vice versa.

The secular RSE pattern and Ediacaran–early Cambrian ocean redox evolution

To further demonstrate the global ocean redox history, we compiled the RSE data from the Wuhe section and other Ediacaran–early Cambrian (ca. 635–520 Ma) anoxic/euxinic shales (Fig. 4 and Table S2) in South China (Goldberg *et al.*, 2007; Guo *et al.*, 2007; Scott *et al.*, 2008; Chang *et al.*, 2010, 2012; Li *et al.*, 2010; Sahoo *et al.*, 2012; Pi *et al.*, 2013; Feng *et al.*, 2014; Chen *et al.*, 2015a; Wang *et al.*, 2015; Wen *et al.*, 2015) and other sedimentary basins (Ugidos *et al.*, 1997; Yu *et al.*, 2009; Johnston *et al.*, 2013; Chen *et al.*, 2015a; Kurzweil *et al.*, 2015). We used the ages of ca. 635 and 632 Ma (the basal Doushantuo Formation; Condon *et al.*, 2005), ca. 580 Ma (Doushantuo Member II–III boundary), ca. 560 Ma (Doushantuo Member IV), ca. 551 Ma (the Miaohe Member; Condon *et al.*, 2005), ca. 542 and 536 Ma (Liuchapo Formation; Chen *et al.*, 2009, 2015b), ca. 532 Ma (Jiang *et al.*, 2009), and ca. 522 Ma (basal Niutitang Formation; Wang *et al.*, 2012a; Chen *et al.*, 2015b) as anchors to constrain the age of individual data points from the South China sections. For the other Ediacaran–early Cambrian successions, we used the age model reported by individual authors.

The compiled RSE data (Fig. 4) reveal modern-level RSE enrichments at ca. 635, ca. 580, ca. 560, ca. 540, ca. 530, and ca. 522 Ma; each of these enrichments is followed by crustal or near-crustal RSE values. A precise estimation of the duration of each oxygenation event requires better geochronological framework, but the relatively thin stratigraphic thicknesses of these events roughly constrains their duration at <5–10 Ma. This secular RSE pattern highlights the presence of rises and falls in the surface oxidation state leading up to the Cambrian explosion. Importantly, this pattern is in direct contrast with a recent view that the Ediacaran–Cambrian ocean was not characterized by statistically significant changes in oxygen content (Sperling *et al.*, 2015). The conclusion of a redox-static and dominantly anoxic Ediacaran–Cambrian ocean (Sperling *et al.*, 2015) is drawn from iron speciation data, which are essentially a local redox proxy (e.g., Lyons *et al.*, 2009) with low statistical probability of robustly capturing the global, mostly unsampled, redox landscape. Our approach, in contrast, relies on local measurements that are impacted by the global inventories of redox sensitive elements, which, in turn, are controlled by the global redox state of the ocean. The RSE method works much in the same way that local carbon isotope measurements in carbonate rocks can capture the global extent of organic carbon burial.

The secular RSE pattern may help explain the delay between the initial appearance of metazoans and the much later appearance and diversification of most metazoan groups until the Cambrian (Fig. 4). Of particular relevance, after the ocean oxygenation event at ca. 635 Ma, extremely low diversification rates (Erwin *et al.*, 2011; Xiao, 2014) and a drop in acritarch diversity (Cohen *et al.*, 2009; Mcfadden *et al.*, 2009) seen in the fossil record between 630 and 580 Ma (Fig. 4) are potentially tied to significant global expansion of reducing conditions unfavorable for animals and complex ecosystems. Definitive mobile bilaterians did not appear until ca. 575 Ma or later (Narbonne, 2004, 2005; Xiao & Laflamme, 2009; Chen *et al.*, 2014; Droser & Gehling, 2015), after our second and third oxygenation events at ca. 580 and ca. 560 Ma, respectively. The frequency of oxygenation events expressed in our data increases during the late Ediacaran–early Cambrian, coincident with the evolution of biomineralizing animals and predatory animals. In this light, we speculate that the ocean oxygenation events in an otherwise anoxic and ecologically monotonous Ediacaran ocean may have stimulated biotic innovations followed by prolonged evolutionary stasis after each event.

CONCLUSION

Integrated data for Fe speciation analysis, S isotope patterns in pyrite, and redox-sensitive elements from euxinic shales of a deep-water slope section in the Yangtze platform, South China, document multiple oxygenation events in an overall anoxic Ediacaran ocean. These oxygenation events may have triggered biotic innovations, separated by prolonged intervals of evolutionary stasis. The rises and falls in the surface oxidation state contrast with the recent view of a redox-static Ediacaran–Cambrian ocean dominated by anoxia and without significant changes in oxygen content. Furthermore, the highly dynamic Ediacaran redox history presented here provides a potential explanation for seemingly conflicting estimates for the timing of Ediacaran ocean oxygenation now present in the literature. This conceptual model also helps to explain the delay between the initial appearance of metazoans and the much later appearance and diversification of most metazoan groups in the early Cambrian.

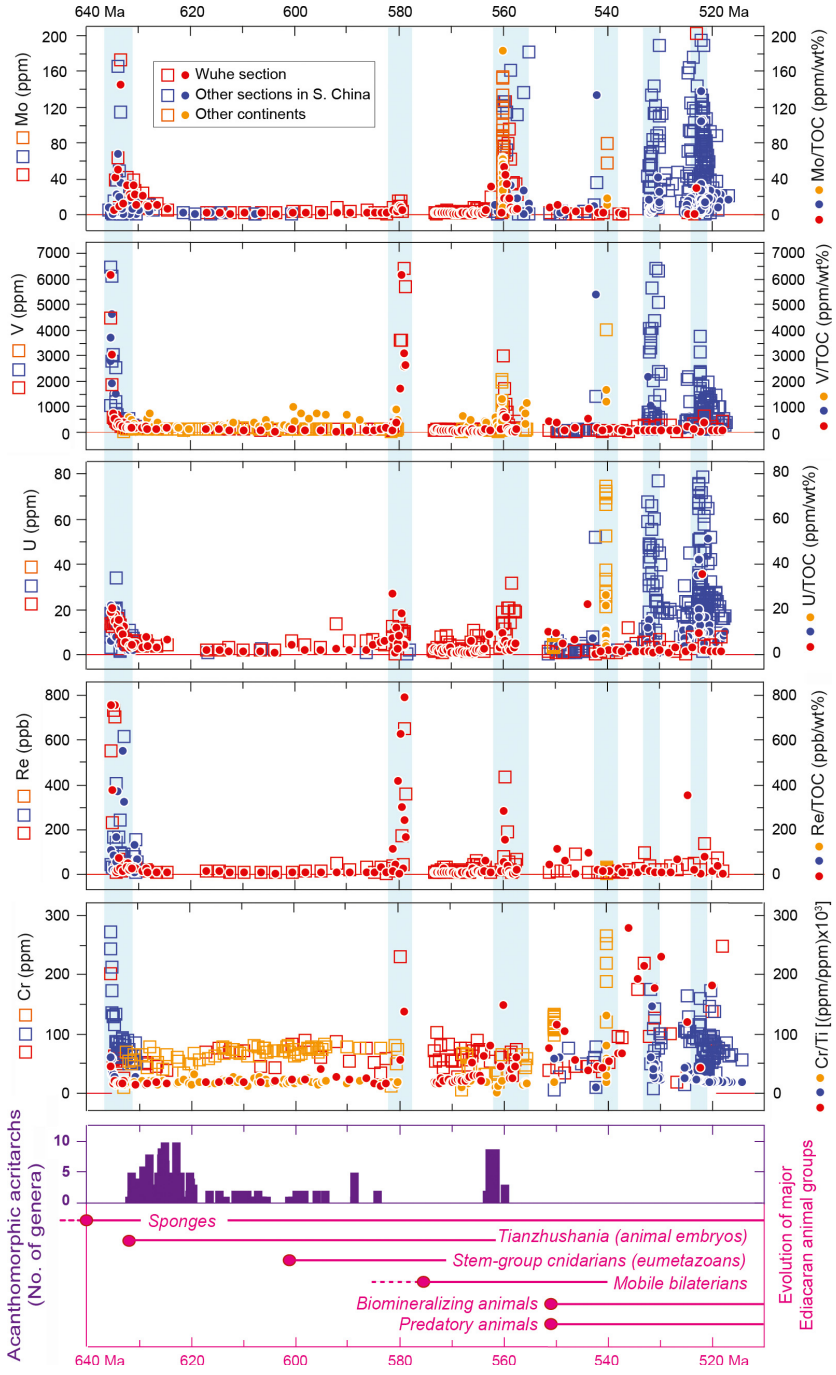

Fig. 4 Compilation of RSE data from the Wuhe section and other Ediacaran–early Cambrian euxinic shales (data are included in Table S2). For Mo, only data from euxinic shales are plotted. For V, U, Re, and Cr, anoxic (ferruginous) and euxinic shales are plotted. The data show multiple oxygenation events in an overall anoxic Ediacaran–early Cambrian ocean. This secular RSE pattern does not support the recent view of a redox-static Ediacaran–Cambrian ocean without statistically significant change in oxygen content (Sperling *et al.*, 2015). Prolonged anoxia between ca. 630 and ca. 580 Ma corresponds with a low diversity of acanthomorphic acritarchs (Cohen *et al.*, 2009; Mcfadden *et al.*, 2009) and delayed diversification of major Ediacaran animal groups (Narbonne, 2004, 2005; Pecoits *et al.*, 2012; Xiao, 2014).

ACKNOWLEDGMENTS

This research was funded by the National Science Foundation Division of Earth Science, the National Natural Science Foundation of China, the NASA Exobiology Program, and the NASA Astrobiology Institute. We thank D. Tang and Y. Wang for field assistance, C. T. Reinhard, C. Scott, L. M. Och, and S. Xiao for helpful discussions, and S. Bates and G. W. Gordon for assistance with laboratory analyses.

AUTHOR CONTRIBUTIONS

The research was designed by G. Jiang, T. W. Lyons, A. D. Anbar, and X. Shi. Samples were collected by S. K. Sahoo, X. Wang, and G. Jiang. Manuscript was prepared by G. Jiang, N. J. Planavsky, S. K. Sahoo, and T. W. Lyons, with important contributions from all co-authors. Analyses were carried out by S. K. Sahoo with contributions from N. J. Planavsky, B. Kendall, and J. D. Owens.

REFERENCES

Algeo TJ, Lyons TW (2006) Mo-total organic carbon covariation in modern anoxic marine environments: implications for analysis of paleoredox and paleohydrographic conditions. *Paleoceanography*, **21**, PA1016.

Algeo TJ, Tribovillard N (2009) Environmental analysis of paleoceanographic systems based on molybdenum–uranium covariation. *Chemical Geology* **268**, 211–225.

An Z, Jiang G, Tong J, Tian L, Ye Q, Song H, Song H (2015) Stratigraphic position of the Ediacaran Miaohe biota and its constrains on the age of the upper Doushantuo δ13C anomaly in the Yangtze Gorges area, South China. *Precambrian Research* **271**, 243–253.

Bristow TF, Kennedy MJ, Derkowski A, Droser M, Jiang G, Creaser RA (2009) Mineralogical constraints on the paleoenvironments of the Ediacaran Doushantuo Formation. *Proceedings of the National Academy of Sciences, USA*, **106**, 13190–13195.

Canfield DE, Poulton SW, Narbonne GM (2007) Late-Neoproterozoic deep-ocean oxygenation and the rise of animal life. *Science* **315**, 92–95.

Canfield DE, Poulton SW, Knoll AH, Narbonne GM, Ross G, Goldberg T, Strauss H (2008) Ferruginous conditions dominated later Neoproterozoic deep-water chemistry. *Science* **321**, 949–952.

Chang HJ, Chu XL, Feng LJ, Huang J (2010) Iron speciation in cherts from the Laobao Formation, South China: implications for anoxic and ferruginous deep-water conditions. *Chinese Science Bulletin* **55**, 3189–3196.

Chang H-J, Chu X-L, Feng L-J, Huang J (2012) Progressive oxidation of anoxic and ferruginous deep-water during deposition of the terminal Ediacaran Laobao Formation in South China. *Palaeogeography, Palaeoclimatology, Palaeoecology* **321**, 80–87.

Chen D, Wang J, Qing H, Yan D, Li R (2009) Hydrothermal venting activities in the Early Cambrian, South China: petrological, geochronological and stable isotopic constraints. *Chemical Geology* **258**, 168–181.

Chen Z, Zhou C, Xiao S, Wang W, Guan C, Hua H, Yuan X (2014) New Ediacara fossils preserved in marine limestone and their ecological implications. *Scientific Reports* **4**, 4180–4190.

Chen X, Ling H-F, Vance D, Shields-Zhou GA, Zhu M, Poulton SW, Och LM, Jiang S-Y, Li D, Cremonese L, Archer C (2015a) Rise to modern levels of ocean oxygenation coincided with the Cambrian radiation of animals. *Nature Communications* **6**, 7142. doi: 10.1038/ncomms8142.

Chen D, Zhou X, Fu Y, Wang J, Yan D (2015b) New U–Pb zircon ages of the Ediacaran–Cambrian boundary strata in South China. *Terra Nova* **27**, 62–68.

Cohen PA, Knoll AH, Kodner RB (2009) Large spinose microfossils in Ediacaran rocks as resting stages of early animals. *Proceedings of the National Academy of Sciences* **106**, 6519–6524.

Condon D, Zhu M, Bowring S, Wang W, Yang A, Jin Y (2005) U–Pb ages from the neoproterozoic Doushantuo Formation, China. *Science* **308**, 95–98.

Cui H, Kaufman AJ, Xiao S, Zhu M, Zhou C, Liu X-M (2015) Redox architecture of an Ediacaran ocean margin: integrated chemostratigraphic ($\delta^{13}C$–$\delta^{34}S$–$^{87}Sr/^{86}Sr$–Ce/Ce*) correlation of the Doushantuo Formation, South China. *Chemical Geology* **405**, 48–62.

Droser ML, Gehling JG (2015) The advent of animals: the view from the Ediacaran. *Proceedings of the National Academy of Sciences* **112**, 4865–4870.

Emerson SR, Huested SS (1991) Ocean anoxia and the concentrations of molybdenum and vanadium in seawater. *Marine Chemistry* **34**, 177–196.

Erwin DH, Laflamme M, Tweedt SM, Sperling EA, Pisani D, Peterson KJ (2011) The Cambrian conundrum: early divergence and later ecological success in the early history of animals. *Science* **334**, 1091–1097.

Feng L, Li C, Huang J, Chang H, Chu X (2014) A sulfate control on marine mid-depth euxinia on the early Cambrian (ca. 529 Ma) Yangtze platform, South China. *Precambrian Research* **246**, 123–133.

Goldberg T, Strauss H, Guo Q, Liu C (2007) Reconstructing marine redox conditions for the Early Cambrian Yangtze Platform: evidence from biogenic sulphur and organic carbon isotopes. *Palaeogeography, Palaeoclimatology, Palaeoecology* **254**, 175–193.

Gomes ML, Hurtgen MT (2015) Sulfur isotope fractionation in modern euxinic systems: implications for paleoenvironmental reconstructions of paired sulfate–sulfide isotope records. *Geochimica et Cosmochimica Acta* **157**, 39–55.

Guo Q, Shields GA, Liu C, Strauss H, Zhu M, Pi D, Goldberg T, Yang X (2007) Trace element chemostratigraphy of two Ediacaran–Cambrian successions in South China: implications for organosedimentary metal enrichment and silicification in the Early Cambrian. *Palaeogeography, Palaeoclimatology, Palaeoecology* **254**, 194–216.

Hetzel A, Böttcher ME, Wortmann UG, Brumsack H (2009) Paleo-redox conditions during OAE 2 reflected in Demerara Rise sediment geochemistry (ODP Leg 207). *Palaeogeography, Palaeoclimatology, Palaeoecology* **273**, 302–328.

Jiang G, Sohl LE, Christie-Blick N (2003) Neoproterozoic stratigraphic comparison of the Lesser Himalaya (India) and Yangtze Block (South China); paleogeographic implications. *Geology* **31**, 917–920.

Jiang G, Kennedy MJ, Christie-Blick N, Wu H, Zhang S (2006) Stratigraphy, sedimentary structures, and textures of the late Neoproterozoic Doushantuo cap carbonate in South China. *Journal of Sedimentary Research* **76**, 978–995.

Jiang G, Kaufman AJ, Christie-Blick N, Zhang S, Wu H (2007) Carbon isotope variability across the Ediacaran Yangtze platform in South China: implications for a large surface-to-deep ocean [delta]13C gradient. *Earth and Planetary Science Letters* **261**, 303–320.

Jiang S-Y, Pi D-H, Heubeck C, Frimmel H, Liu Y-P, Deng H-L, Ling H-F, Yang J-H (2009) Early Cambrian ocean anoxia in South China. *Nature* **459**, E5–E6.

Jiang G, Shi X, Zhang S, Wang Y, Xiao S (2011) Stratigraphy and paleogeography of the Ediacaran Doushantuo Formation (ca. 635–551 Ma) in South China. *Gondwana Research* **19**, 831–849.

Johnston DT, Poulton SW, Tosca NJ, O'brien T, Halverson GP, Schrag DP, Macdonald FA (2013) Searching for an oxygenation event in the fossiliferous Ediacaran of northwestern Canada. *Chemical Geology*, **362**, 273–286.

Kendall B, Reinhard CT, Lyons TW, Kaufman AJ, Poulton SW, Anbar AD (2010) Pervasive oxygenation along late Archaean ocean margins. *Nature Geoscience* **3**, 647–652.

Kendall B, Komiya T, Lyons TW, Bates SM, Gordon GW, Romaniello SJ, Jiang G, Creaser RA, Xiao S, Mcfadden K, Sawaki Y, Tahata M, Shu D, Han J, Li Y, Chu X, Anbar AD (2015) Uranium and molybdenum isotope evidence for an episode of widespread ocean oxygenation during the late Ediacaran Period. *Geochimica et Cosmochimica Acta* **156**, 173–193.

Knoll AH (2011) The multiple origins of complex multicellularity. *Annual Review of Earth and Planetary Sciences* **39**, 217–239.

Knoll AH, Carroll SB (1999) Early animal evolution: emerging views from comparative biology and geology. *Science* **284**, 2129–2137.

Kurzweil F, Drost K, Pašava J, Wille M, Taubald H, Schoeckle D, Schoenberg R (2015) Coupled sulfur, iron and molybdenum isotope data from black shales of the Teplá–Barrandian unit argue against deep ocean oxygenation during the Ediacaran. *Geochimica et Cosmochimica Acta* **171**, 121–142.

Large RR, Halpin JA, Danyushevsky LV, Maslennikov VV, Bull SW, Long JA, Gregory DD, Lounejeva E, Lyons TW, Sack PJ, Mcgoldrick PJ, Calver CR (2014) Trace element content of sedimentary pyrite as a new proxy for deep-time ocean–atmosphere evolution. *Earth and Planetary Science Letters* **389**, 209–220.

Leavitt WD, Halevy I, Bradley AS, Johnston DT (2013) Influence of sulfate reduction rates on the Phanerozoic sulfur isotope record. *Proceedings of the National Academy of Sciences* **110**, 11244–11249.

Li C, Love GD, Lyons TW, Fike DA, Sessions AL, Chu X (2010) A stratified redox model for the Ediacaran ocean. *Science* **328**, 80–83.

Liu P, Yin C, Chen S, Tang F, Gao L (2013) The biostratigraphic succession of acanthomorphic acritarchs of the Ediacaran Doushantuo Formation in the Yangtze Gorges area, South China and its biostratigraphic correlation with Australia. *Precambrian Research* **225**, 29–43.

Love GD, Grosjean E, Stalvies C, Fike DA, Grotzinger JP, Bradley AS, Kelly AE, Bhatia M, Meredith W, Snape CE, Bowring SA, Condon DJ, Summons RE (2009) Fossil steroids record the appearance of Demospongiae during the Cryogenian period. *Nature* **457**, 718–721.

Lyons TW, Severmann S (2006) A critical look at iron paleoredox proxies based on new insights from modern euxinic marine basins. *Geochimica et Cosmochimica Acta* **70**, 5698–5722.

Lyons TW, Anbar AD, Severmann S, Scott C, Gill BC (2009) Tracking euxinia in the ancient ocean: a multiproxy perspective and Proterozoic case study. *Annual Review of Earth and Planetary Sciences* **37**, 507–534.

Lyons TW, Reinhard CT, Planavsky NJ (2014) The rise of oxygen in Earth/'s early ocean and atmosphere. *Nature* **506**, 307–315.

Mcfadden KA, Huang J, Chu X, Jiang G, Kaufman AJ, Zhou C, Yuan X, Xiao S (2008) Pulsed oxidation and biological evolution in the Ediacaran Doushantuo Formation. *Proceedings of the National Academy of Sciences of the United States of America* **105**, 3197–3202.

Mcfadden KA, Xiao S, Zhou C, Kowalewski M (2009) Quantitative evaluation of the biostratigraphic distribution of acanthomorphic acritarchs in the Ediacaran Doushantuo Formation in the Yangtze Gorges area, South China. *Precambrian Research* **173**, 170–190.

McLennan SM (2001) Relationships between the trace element composition of sedimentary rocks and upper continental crust. *Geochemistry, Geophysics, Geosystems* **2**, 2000GC000109, doi:10.1029/2000GC000109.

Narbonne GM (2004) Modular construction of early Ediacaran complex life forms. *Science* **305**, 1141–1144.

Narbonne GM (2005) The Ediacara biota: Neoproterozoic origin of animals and their ecosystems. *Annual Review of Earth and Planetary Sciences* **33**, 421–442.

Och LM, Shields-Zhou GA (2012) The Neoproterozoic oxygenation event: environmental perturbations and biogeochemical cycling. *Earth-Science Reviews* **110**, 26–57.

Och LM, Cremonese L, Shields-Zhou GA, Poulton SW, Struck U, Ling H, Li D, Chen X, Manning C, Thirlwall M, Strauss H, Zhu M (2015) Palaeoceanographic controls on spatial redox distribution over the Yangtze Platform during the Ediacaran–Cambrian transition. *Sedimentology*, in press.

Owens JD, Lyons TW, Li X, Macleod KG, Gordon G, Kuypers MMM, Anbar A, Kuhnt W, Severmann S (2012) Iron isotope and trace metal records of iron cycling in the proto-North Atlantic during the Cenomanian–Turonian oceanic anoxic event (OAE-2). *Paleoceanography* **27**, PA3223, doi:10.1029/2012PA00232.

Pecoits E, Konhauser KO, Aubet NR, Heaman LM, Veroslavsky G, Stern RA, Gingras MK (2012) Bilaterian burrows and grazing behavior at >585 million years ago. *Science* **336**, 1693–1696.

Pi D-H, Liu C-Q, Shields-Zhou GA, Jiang S-Y (2013) Trace and rare earth element geochemistry of black shale and kerogen in the early Cambrian Niutitang Formation in Guizhou province, South China: constraints for redox environments and origin of metal enrichments. *Precambrian Research* **225**, 218–229.

Poulton SW, Canfield DE (2005) Development of a sequential extraction procedure for iron: implications for iron partitioning in continentally derived particulates. *Chemical Geology* **202**, 79–94.

Poulton SW, Canfield DE (2011) Ferruginous conditions: a dominant feature of the ocean through Earth's History. *Elements* **7**, 107–112.

Reinhard CT, Planavsky NJ, Robbins LJ, Partin CA, Gill BC, Lalonde SV, Bekker A, Konhauser KO, Lyons TW (2013) Proterozoic ocean redox and biogeochemical stasis. *Proceedings of the National Academy of Sciences* **110**, 5357–5362.

Sahoo SK, Planavsky NJ, Kendall B, Wang X, Shi X, Scott C, Anbar AD, Lyons TW, Jiang G (2012) Ocean oxygenation in the wake of the Marinoan glaciation. *Nature* **489**, 546–549.

Sawaki Y, Ohno T, Tahata M, Komiya T, Hirata T, Maruyama S, Windley BF, Han J, Shu D, Li Y (2010) The Ediacaran radiogenic Sr isotope excursion in the Doushantuo Formation in the Three Gorges area, South China. *Precambrian Research* **176**, 46–64.

Scott C, Lyons TW, Bekker A, Shen Y, Poulton SW, Chu X, Anbar AD (2008) Tracing the stepwise oxygenation of the Proterozoic ocean. *Nature* **452**, 456–459.

Scott C, Wing BA, Bekker A, Planavsky NJ, Medvedev P, Bates SM, Yun M, Lyons TW (2014) Pyrite multiple-sulfur isotope evidence for rapid expansion and contraction of the early Paleoproterozoic seawater sulfate reservoir. *Earth and Planetary Science Letters* **389**, 95–104.

Sperling EA, Frieder CA, Raman AV, Girguis PR, Levin LA, Knoll AH (2013) Oxygen, ecology, and the Cambrian radiation of animals. *Proceedings of the National Academy of Sciences* **110**, 13446–13451.

Sperling EA, Wolock CJ, Morgan AS, Gill BC, Kunzmann M, Halverson GP, Macdonald FA, Knoll AH, Johnston DT (2015) Statistical analysis of iron geochemical data suggests limited late Proterozoic oxygenation. *Nature* **523**, 451–454.

Tahata M, Ueno Y, Ishikawa T, Sawaki Y, Murakami K, Han J, Shu D, Li Y, Guo J, Yoshida N, Komiya T (2012) Carbon and oxygen isotope chemostratigraphies of the Yangtze platform, South China: decoding temperature and environmental changes through the Ediacaran. *Gondwana Research* **23**, 333–353.

Tribovillard N, Algeo TJ, Lyons T, Riboulleau A (2006) Trace metals as paleoredox and paleoproductivity proxies: An update. *Chemical Geology* **232**, 12–32.

Ugidos JM, Armenteros I, Barba P, Valladares MI, Colmenero JR (1997) Geochemistry and petrology of recycled orogen-derived sediments: a case study from Upper Precambrian siliciclastic rocks of the Central Iberian Zone, Iberian Massif, Spain. *Precambrian Research* **84**, 163–180.

Wang X, Shi X, Jiang G, Zhang W (2012a) New U–Pb age from the basal Niutitang Formation in South China: implications for diachronous development and condensation of stratigraphic units across the Yangtze platform at the Ediacaran–Cambrian transition. *Journal of Asian Earth Sciences* **48**, 1–8.

Wang L, Shi X, Jiang G (2012b) Pyrite morphology and redox fluctuations recorded in the Ediacaran Doushantuo Formation. *Palaeogeography, Palaeoclimatology, Palaeoecology* **333–334**, 218–227.

Wang X, Shi X, Zhao X, Tang D (2015) Increase of seawater Mo inventory and ocean oxygenation during the early Cambrian. *Palaeogeography, Palaeoclimatology, Palaeoecology* **440**, 621–631.

Wen H, Fan H, Zhang Y, Cloquet C, Carignan J (2015) Reconstruction of early Cambrian ocean chemistry from Mo isotopes. *Geochimica et Cosmochimica Acta* **164**, 1–16.

Wilkin RT, Arthur MA, Dean WE (1997) History of water-column anoxia in the Black Sea indicated by pyrite framboid size distributions. *Earth and Planetary Science Letters* **148**, 517–525.

Xiao S (2014) Oxygen and early animal evolution. In *Treatise on Geochemistry*, 2nd edn. (ed. Farquhar J). Elsevier, Dordrecht, pp. 231–250.

Xiao S, Laflamme M (2009) On the eve of animal radiation: phylogeny, ecology and evolution of the Ediacara biota. *Trends in Ecology & Evolution* **24**, 31–40.

Yin L, Zhu M, Knoll AH, Yuan X, Zhang J, Hu J (2007) Doushantuo embryos preserved inside diapause egg cysts. *Nature* **446**, 661–663.

Yu B, Dong H, Widom E, Chen J, Lin C (2009) Geochemistry of basal Cambrian black shales and cherts from the Northern Tarim Basin, Northwest China: implications for depositional setting and tectonic history. *Journal of Asian Earth Sciences* **34**, 418–436.

Zhang S, Jiang G, Zhang J, Song B, Kennedy MJ, Christie-Blick N (2005) U–Pb sensitive high-resolution ion microprobe ages from the Doushantuo Formation in south China: constraints on late Neoproterozoic glaciations. *Geology* **33**, 473–476.

Zhang S, Evans DAD, Li H, Wu H, Jiang G, Dong J, Zhao Q, Raub TD, Yang T (2013) Paleomagnetism of the late Cryogenian Nantuo Formation and paleogeographic implications for the South China Block. *Journal of Asian Earth Sciences* **72**, 164–177.

Zhang S, Li H, Jiang G, Evans DAD, Dong J, Wu H, Yang T, Liu P, Xiao Q (2015) New paleomagnetic results from the Ediacaran Doushantuo Formation in South China and their paleogeographic implications. *Precambrian Research* **259**, 130–142.

Zhou C, Xiao S (2007) Ediacaran $\delta^{13}C$ chemostratigraphy of South China. *Chemical Geology* **237**, 89–108.

Zhou C, Xie G, Mcfadden K, Xiao S, Yuan X (2007) The diversification and extinction of Doushantuo–Pertatataka acritarchs in South China: causes and biostratigraphic significance. *Geological Journal* **42**, 229–262.

Zhu M, Zhang J, Yang A (2007) Integrated Ediacaran (Sinian) chronostratigraphy of South China. *Palaeogeography, Palaeoclimatology, Palaeoecology* **254**, 7–61.

Zhu M, Lu M, Zhang J, Zhao F, Li G, Aihua Y, Zhao X, Zhao M (2013) Carbon isotope chemostratigraphy and sedimentary facies evolution of the Ediacaran Doushantuo Formation in western Hubei, South China. *Precambrian Research* **225**, 7–28.

SUPPORTING INFORMATION

Additional Supporting Information may be found in the online version of this article:

Table S1. Iron speciation, sulfur isotope, and trace element data from the Wuhe section (used for Fig. 2).

Table S2. Compiled geochemical data from Ediacaran–early Cambrian black shales (ca. 635–520 Ma) used for Fig. 4.